Saleemsab Doddamani[1], *Mohamed Kaleemulla*[2]

EFFECT OF GRAPHITE ADDITION ON THE FRACTURE AND FATIGUE CRACK GROWTH BEHAVIOUR OF Al6061-GRAPHITE

UTICAJ DODATKA GRAFITA NA LOM I RAST ZAMORNE PRSLINE KOD Al6061-GRAFITA

Originalni naučni rad / Original scientific paper
UDK /UDC: 66.018.9:539.42

Rad primljen / Paper received: 1.11.2018

Adresa autora / Author's address:
1) Department of Mechanical Engineering, Jain Polytechnic, Davangere, Karnataka, India email: saleemsabdoddamani@gmail.com
2) Department of Studies in Mechanical Engineering, University BDT College of Engineering, Karnataka, India

Keywords
- Al6061-graphite composites
- FCGR
- S-N curve
- CT specimens

Abstract

Nowadays in industries, especially in aerospace industries life prediction method is based on fracture mechanics. In the fracture mechanics model, it is expected that an initial crack which grows from voids exists in the specimen. CT specimens are made of Al6061-graphite particulate composites with 9 % of graphite reinforcement. For the same composition, three different orientations are considered with B = 10 mm, W = 40 mm to estimate the fatigue crack growth rate, and to study the fatigue life cycle through the stress-life cycle. The threshold value for Al6061-9% graphite at an R = 0.1 is found to be between 3.5 to 3.75 MPa√m. From the trend of the stress-life cycle curve, it is clear that the fatigue life of the composite achieves the level of 10^5 *when the stress amplitude is lower than 250 MPa.*

Ključne reči
- Al6061-grafitni kompozit
- FCGR (brzina rasta zamorne prsline)
- krive zamaranja
- CT epruvete

Izvod

U današnje vreme, posebno u aerokosmičkoj industriji metoda procene veka se zasniva na mehanici loma. Kod modela mehanike loma, očekuje se prisustvo inicijalne prsline koja raste iz šupljina u uzorcima. CT epruvete su izrađene od Al6061-grafitnih čestičnih kompozita sa 9 % grafitnog ojačanja. Pri istom sastavu, razmatraju se tri različite orijentacije sa B = 10 mm, W = 40 mm u cilju procene brzine rasta zamorne prsline, i proučavanja ciklusa veka zamaranja prema ciklusu napona-veka. Granična vrednost kod Al6061-9 % grafita pri R = 0,1 se nalazi u granicama između 3,5 do 3,75 MPa√m. Prema karakteru krive napon-ciklus veka, jasno je da zamorni vek kompozita dostiže nivo od 10^5 *kada je amplituda napona manja od 250 MPa.*

INTRODUCTION

Fracture toughness is typically utilized as a general phrase for measures of material imperviousness to crack propagation. Values of fracture toughness may likewise serve as a premise in performance evaluation, quality affirmation and material description for representative engineering structures, together with oil and gas pipelines, aircraft, ship and automotive structures, piping and pressure vessels, petrochemical tanks etc. In this manner, fracture toughness investigation and assessment have been a critical issue being developed for fracture mechanics technique and its engineering applications. The most important parameters /1/ used in fracture mechanics are the elastic energy release rate G (or its equivalent accomplice - stress intensity factor K), the J-integral and the crack-tip opening displacement (CTOD). To measure these parameters many experimental techniques have been adopted to explain the material's fracture toughness (K_{Ic}). Customary terminology relating to K_{Ic} testing and assessment is defined in E399-17 /2/ by the American Society for Testing and Materials (ASTM).

All concepts and requisites relating to fracture tests utilized as a part of this work are characterized by ASTM E399. ASTM /1/ fracture test standards prescribe many types of conventional fracture test specimens. These include single edge-notch bend (SENB) specimen, compact tension (CT) specimen, disk-shaped compact tension (DCT) specimen, arc-shaped bend (AB) specimen and arc-shaped tension (AT) specimen. Different specimen size requirements are prescribed for different fracture test standards so as to get valid fracture toughness, also to restrict the effects of crack-tip limitation on that fracture toughness parameter.

Eun E. Lee /4/ worked on the fatigue performance of Al-SiC composites, R. Yuan et al. /5/ conducted fracture toughness and cyclic fatigue tests on Al-SiC ceramics, Abdul Budan et al /6/ investigated fatigue and mechanical properties of Al6061 alloy reinforced with silicon carbide and graphite particles, Y. Uematsu /7/ conducted fatigue tests at elevated temperature using smooth specimens of SiC-particulate-reinforced aluminium alloy composites with different particle sizes at a constant wt.% of SiC particles, D.P. Myriounis et al. /8/ examined fatigue and fracture toughness behaviour of aluminium reinforced with SiC particles. J. Huang et al. /9/ studied microstructural variability on the very high-cycle fatigue behaviour of discontinuously-reinforced SiCp aluminium MMCs. M.M. Sharma et al. /10/ studied fatigue characteristics of SiCp reinforced spray-formed 7XXX series aluminium alloys. Experimental results of the authors reveal the enhancement in fatigue and fracture behaviour of the material. Bikash Joadder et al. /11/ failure cycles. A.R. Shahani et al. /12/ utilized compact tension specimens to estimate the methods in fatigue life prediction. Similar experiments were conducted by many researchers /13, 14/ for fatigue life prediction.

Nowadays in industries, especially in aerospace industries, life prediction method is based on fracture mechanics. In numerous global associations, for example, ASTM, NASA, etc., fracture mechanics based life prediction /12/ is the primary region of research. In the fracture mechanics model, it is expected that an initial crack which grows from voids exists in the specimen. The voids in the industrial component are the defects that occur in manufacture.

With the arrival of fracture mechanics /13/, an additional motivated job is embraced, i.e., to forecast the crack propagation. It obviously becomes known that the 'speed' of propagation is a long way from being steady in time: initially the Irwin stress intensity factor is used to characterize the crack growth rate per cycle (*da/dN*) until the revolutionary work of Paris and others. From that point forward, to obtain the more from the Paris' law /14/ and its deviations, additional research has been made; however, we are still a long way from total comprehension.

Apart from the ideal conditions, Paris' law deals only with single mechanisms of a different approach: threshold limits, crack closure, short cracks, both fatigue limit and crack propagation threshold. The instance of short cracks is a standout amongst the most surely understood since Paris' law can considerably underrate their development; on the other hand, a significant number of laws reflect that there isn't a single kind of short-crack deviation. A few authors have recommended a classification of cracks as takes after:

- Microscopic short crack (microstructurally small).
- Mechanically small crack (physically little) contrasted with the size of plasticity region, for which elastic-plastic fracture mechanics (EPFM) is required.
- Macroscopic long crack, development stage illustrated by linear elastic fracture mechanics (LEFM).

In fracture mechanics approach, the Paris model is used to determine life cycles such as Eq.(1):

$$N_f = \int_{a_i}^{a_f} \frac{da}{C(\Delta K)^m} \tag{1}$$

where: C and m are Paris' law parameters.

In Eq.(1), integrals' maximal point of confinement can be computed by the fracture toughness of the material. Then again, the computing of the initial crack length (a_i) is one of the issues of this technique, /12/. The initial crack length or initial flaw size (IFS) can be measured by Non-Destructive Testing (NDT). Despite that, the initial crack length can be underneath the present identification ability of the NDT strategy. In the event that the NDT detection limit is picked as the initial crack length, it will achieve an exceptionally moderate design. Additionally, the conduct of a small crack growth development is convoluted and is dependent on the microstructures of the material.

A reasonable decent agreement is obtained between the proposed correlation /13/ and experimental data concerning aluminium, titanium and steel compounds. J.R. Mohanty et al. /14/ proposed an alternative method to determining the crack growth rate of aluminium alloys. Calculating the crack growth rate from laboratory experimentation is one of the tedious work because of the discrete set of crack length (a) with a change in a number of cycles (N). To reduce the scatter of a large amount of data, data smoothening methods are necessary. An exponential equation has been proposed to calculate the crack growth rate (*da/dN*).

The cyclic stress intensity factor (ΔK) and fatigue crack growth rate (*da/dN*) are determined from the Eqs.(2) and (3), /17/, respectively:

$$\Delta K = \frac{\Delta P}{B\sqrt{W}} f\left(\frac{a}{W}\right), \tag{2}$$

$$\frac{da}{dN} = \frac{(a_j - a_i)}{(N_j - N_i)}, \tag{3}$$

where:

$$f\left(\frac{a}{W}\right) = \frac{\left(2+\frac{a}{W}\right)}{\left(1-\frac{a}{W}\right)^{3/2}}\left[0.886+4.64\left(\frac{a}{W}\right)-13.32\left(\frac{a}{W}\right)^2+\right.$$
$$\left.+14.72\left(\frac{a}{W}\right)^3-5.6\left(\frac{a}{W}\right)^4\right];$$

a_i, a_j = crack length in i-th and j-th step in mm; N_i, N_j = number of cycles in the i-th and j-th step; i = number of experimental steps, and $j = i + 1$.

To calculate whether a crack is fit for developing, the stress intensity range must be determined. If the determined range of stress intensity surpasses the value calculated for the threshold of fatigue, crack development will happen. Fatigue life of the specimens is estimated under different load amplitudes and a stress ratio of 0.1.

Many authors made an attempt for fatigue crack growth and fracture toughness in Al-SiC particulate MMCs. Davidson, et al. /18/, Mason, et al. /19/, Nirbhay Singh, et al. /20/, Xue, et al. /21/, Chawla, et al. /22/, utilize 2XXX aluminium alloy with SiC as a reinforcement to study the fatigue crack growth rate. Most of the authors have investigated the fatigue fracture behaviour and compared it with the fatigue response of the composite.

Other CTOD/CMOD works by various researchers include the construction of CTOD-R curve from surface displacement measurements, /23/, effect CTOD fracture toughness of API X65 steel /24/, fatigue crack growth in SiC particle reinforced Al alloy matrix /25/, crack mouth opening displacement from non-standard fracture test specimens /26/, CTOD for various *a/W* ratios /27/, effect of numerical parameters on plastic CTOD /28/, evaluation of CTOD in constant amplitude fatigue crack growth from crack tip displacement fields /29/, influence of crack tip shielding on fatigue crack propagation /30/.

Finding the fatigue limit or fatigue life of structural members requires the plot of the S-N curve which requires interdependencies resulting from the material information. The S-N curves are utilized as a part of findings for both constrained and boundless fatigue life regimes.

The motivation behind the investigation is to decide the fatigue life and fatigue limit displaying process for constrained and boundless fatigue life regime by experimental plotting the S-N curve. The material, geometry, and load levels are the factors which affect the initiation and propagation of cracks. Fatigue failure will be of high cycle (HCF) numbers at low load levels. In stage-I itself, crack propagation will be nucleated, rather than propagating in stages II and III. Fatigue failure will be of low cycle (LCF) numbers at high load levels in which cyclic plastic deformation happens quickly, prompting failure. These different procedures result in the outstanding empirical Wöhler curve.

Fatigue loading

The capacity of the stress intensity to reflect crack-tip conditions remains scientifically right; however, the connection of ΔK_I to crack development is an effective application by the repeated exhibition. It is fascinating, in any case, to state that the S-N fatigue life curve relies upon the initial crack size, a_i.

$$\Delta\sigma_{th} = \frac{\Delta K_{th}}{\sqrt{\pi a_i}}, \tag{4}$$

where: $\Delta\sigma$ is the stress amplitude; ΔK is the stress intensity range; and a_i is initial crack size.

Many researchers reviewed the fatigue and fracture behaviour of aluminium matrix reinforced with SiCp. The Al/SiC$_p$ composites may be subjected to with- or without heat treatment. The fatigue and fracture toughness behaviour is monitored by many researchers and the resulting stress-life (S-N) curve is experimentally obtained.

In this background, the research gaps indicate that there is a lot of scope for current researchers for investigation with the use of graphite particles as a reinforcing material. Therefore this work will focus on the fracture behaviour of aluminium matrix graphite reinforced MMCs. The objective is to find the threshold fracture toughness (ΔK) of the Al6061-graphite particulate composite by using compact tension (CT) specimens.

MATERIALS AND PROCESSING

Materials

Precipitation-hardened aluminium alloy, called Al6061, and its main alloying elements are silicon (0.70%) and magnesium (0.81%). Physical properties /31/ of Al6061 are hardness 95 BHN, elastic modulus 68.9 GPa, ultimate tensile strength 315 MPa, yield strength 275 MPa, elongation 17%. Graphite is available in the shape of fibres and particles which has been identified as a high strength material. Physical properties of graphite /32/ are elastic modulus 15 GPa, yield strength 55 MPa, the thermal expansion coefficient is 8.2×10^{-6} °C. Out of many factors which influence the fracture properties, the particle size of graphite is the most important microstructural variable. The average graphite particle size is 44 μm.

Al6061 and graphite particulate metal matrix composites produced by solidification techniques present greater tribological properties such as better machinability, low wear rate, high damping capacity, low coefficient of friction, and their outstanding antifriction properties used for a range of automobile applications, /33/.

Al6061 as matrix and graphite particles as reinforcement are utilized for the work. The reason to involve these materials is their density. The density of Al6061 is 2.65 g/cm^3 and of graphite 2.26 g/cm^3. The Al6061-graphite particulate composites exhibit isotropic properties, /34/, and also have outstanding combinations of physical, thermal, mechanical, structural properties.

Processing

The stir casting method /33, 34/ is utilized to prepare the Al6061-graphite particulate metal matrix composites at 9% weight fractions of graphite. The Al6061 blocks are allowed to melt in the stir casting furnace at a temperature about 720 °C. A degasifier has been added to the molten aluminium to remove the gases. The requisite quantity of graphite particles is added to the molten Al6061 while stirring with a stirrer at speed of 500 rpm. In the mold, molten Al6061-graphite is poured, and it is allowed to solidify. After solidification, the solid bars are taken out from the mould. The solid bars are machined as per the specimen requirements for determining required properties of Al6061-graphite composites.

EXPERIMENTATION

To evaluate the initial flaw size (IFS), experimental investigations are carried out on CT specimens prepared by Al6061-graphite particulate composites and the number of cycles is counted, necessary for the crack to propagate from the notched end up to its final length at the beginning of fracture. Machined specimens from the composite block are fabricated to required dimensions as per ASTM standards (shown in Fig. 1). As per the ASTM standard, the notch is prepared by using wire-cut EDM at an accuracy of 0.2 mm. Notch size is 4 mm × 17 mm for all specimens. Further, a fatigue crack is introduced at the end of the notch by maintaining crack length to width ratio $a/W = 0.45$, i.e. fatigue cracks of 1 mm; 1.8 mm; 2 mm have been introduced using a servo-hydraulic testing machine. Fracture toughness experiments are carried out at room temperature in the servohydraulic testing machine with 250 kN load capacity. All specimens are subjected to a load ratio of 0.1 and by maintaining the displacement rate 1 mm/min. Cyclic loading is applied by maintaining the frequency of 5 Hz.

Experiments are conducted for three different orientations, i.e. T-S, L-T, and L-S, where T is the transverse direction, L is the longitudinal direction, and S is the short transverse direction. The first alphabet indicates the direction of the load applied and the second alphabet indicates the direction of crack propagation. The geometry of the CT specimen is given in Fig. 1. Width (W) of the specimens is considered as 40 mm, whereas the thickness (B) of the specimens is 10 mm. Specimens are made of Al6061-graphite particulate composites with 9 % of graphite reinforcement.

The load and displacement plot is shown in Fig. 2. By using an optical method, the crack growth is monitored for all the Al6061-9 % graphite specimens utilizing a COD gauge mounted on the face of the machined notch.

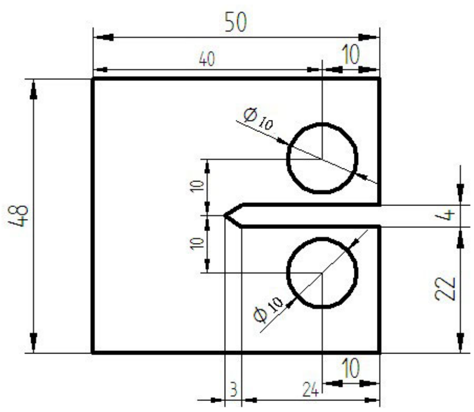

Figure 1. Geometry of the compact tension (CT) specimens.

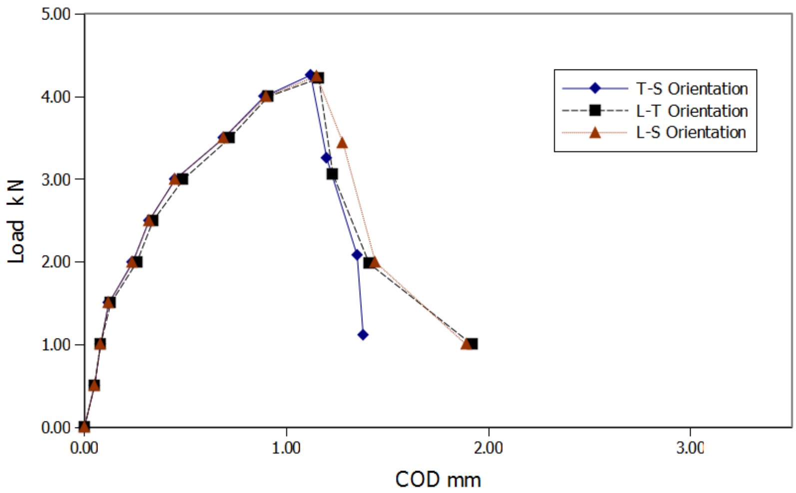

Figure 2. Load and displacement data for different orientations.

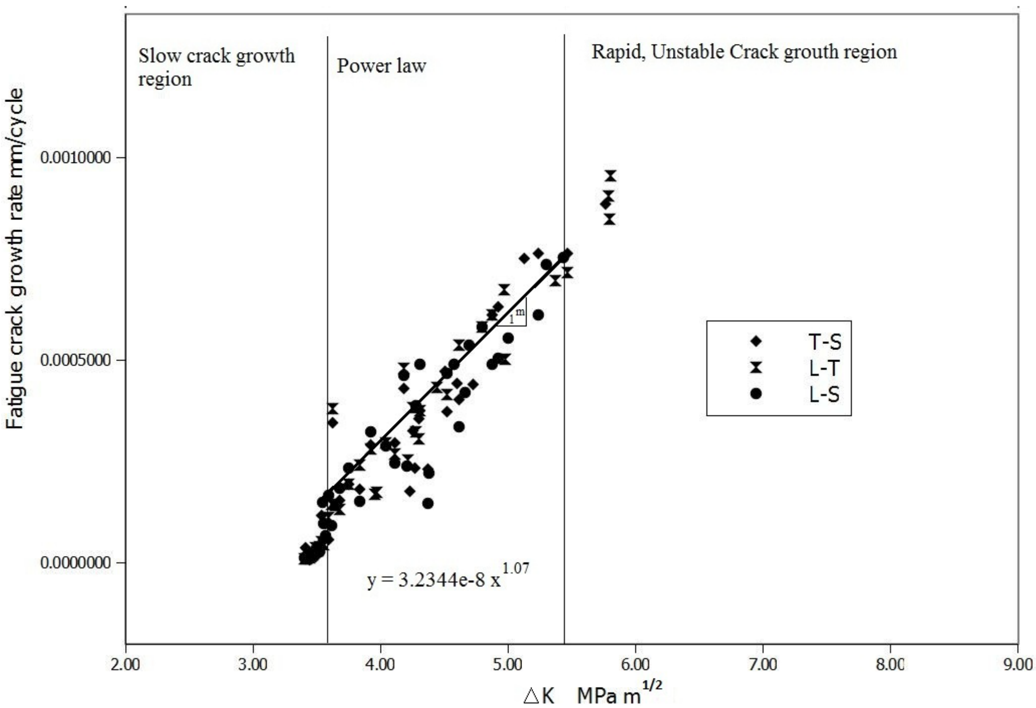

Figure 3. Crack growth rate vs. cyclic stress intensity factor.

For each particular orientation, two specimens are tested and the results displayed are the better of the two specimens considered. However, there is not much difference in the values obtained (the error may be less than 5 %). Fracture load and the calculated value of the fracture toughness of Al6061-9 % graphite MMCs have been listed in Table 1.

Table 1. Fracture toughness of Al6061-9 % graphite MMC for different orientations.

Orientation	a/W	Fracture load (P_Q) kN	$f\{a/W\}$	K_{Ic} MPa$\sqrt{\text{m}}$
T-S	0.45	4.26	8.34	17.76
L-T	0.45	4.22	8.34	17.59
L-S	0.45	4.25	8.34	17.72

From the experimental results, it is clear that in all directions the fracture properties are nearly the same. For the T-S and L-S orientations, the fracture toughness remains the same with negligible error. This may be the result of the addition of graphite particles in the aluminium matrix. The Al6061-graphite composite will become a homogeneous material and it exhibits isotropic properties.

RESULTS AND DISCUSSIONS

Obtained fatigue crack growth data are evaluated and are drawn as shown in Fig. 3. Figure 3 is a combination of all the data points on the crack growth rate vs. cyclic stress intensity factor graph. A linear fitting curve line is drawn through the data points. The equation of this line is $da/dN = (3.2344 \times 10^{-8})\ \Delta K^{1.07}$.

Data points underneath a ΔK of 1.7 MPa√m are not utilized in the determination of these lines as these data points are generally near to the threshold region and are significantly divergent from the rest of the data. The threshold value for Al6061-9 % graphite at an $R = 0.1$ is found to be in between 3.5 to 3.75 MPa√m. Al6061-9 % graphite specimen is cycled at a $\Delta K = 0.3$ MPa√m for 40 000 cycles. It is then cycled at a $\Delta K = 3.70$ MPa√m for 108 000 and crack growth began. Figure 3 demonstrates an approximate vertical region between $\Delta K = 3.5$ to 3.75 MPa√m, indicating the threshold region. The machine time required for the threshold value for Al6061-9 % graphite composite is 2.2 hours (40 000 cycles) and is checked in the development region for 3.2 hours (231 000 cycles), and cumulative time of 5.4 hours.

The Paris coefficients of Al6061-9 % graphite composite MMCs are determined using the fatigue crack growth rate vs. cyclic stress intensity factor (da/dN vs ΔK) diagram, /12/. The best fitting line is drawn to the linear portion of the diagram. The Paris coefficients obtained are as $C = 3.2344 \times 10^{-0.8}$ and $m = 1.07$, which are shown in Fig. 3. The fatigue life forecasted, based on the estimation of the Paris equation technique, is judged against the life calculated by the experimental method, and given in Table 2.

Table 2a. Comparison of fatigue life, T-S orientation.

Sl no	Experimental N_f cycles	Predicted N_p cycles	Error (%)
1	63700	63152	0.86
2	128000	128486	0.37
3	142000	131584	7.33
4	156000	157801	1.14
5	188000	190198	1.15

Table 2b. Comparison of fatigue life, L-T orientation.

Sl no	Experimental N_f cycles	Predicted N_p cycles	Error (%)
1	62000	63152	1.85
2	128300	128486	0.14
3	143000	131584	7.98
4	162000	148244	8.49
5	176000	169167	3.88

Table 2c. Comparison of fatigue life, L-S orientation.

Sl no	Experimental N_f cycles	Predicted N_p cycles	Error (%)
1	63000	63152	0.24
2	128000	128486	0.24
3	142000	131584	7.33
4	165000	170285	3.20
5	189000	190198	0.63

From Table 2, it is clear that there is a good correlation between the experimental and predicted values of the life cycle. For the T-S, L-T, L-S orientations, the predicted life and experimental fatigue life are in good agreement with each other with a deviation of less than 10 %.

The fatigue test of Al6061-9 % graphite is conducted to estimate the fatigue limit of the material. Fatigue test data have been analysed and the S-N curve is plotted. Figure 4 shows the S-N curve of stress amplitude vs. number of cycles to failure of Al6061-9 % graphite particulate composite.

From Fig. 4, it is found that the fatigue life of the MMC is reduced with increasing stress amplitude, for example, the fatigue life of the studied alloy is 2.1×10^5 under stress amplitude of 200 MPa, while about 1.30×10^5 under stress amplitude of 250 MPa. From the trend of the S-N curve it is clear that when the stress amplitude is lower than 250 MPa, the fatigue life of the composite achieves the level of 10^5.

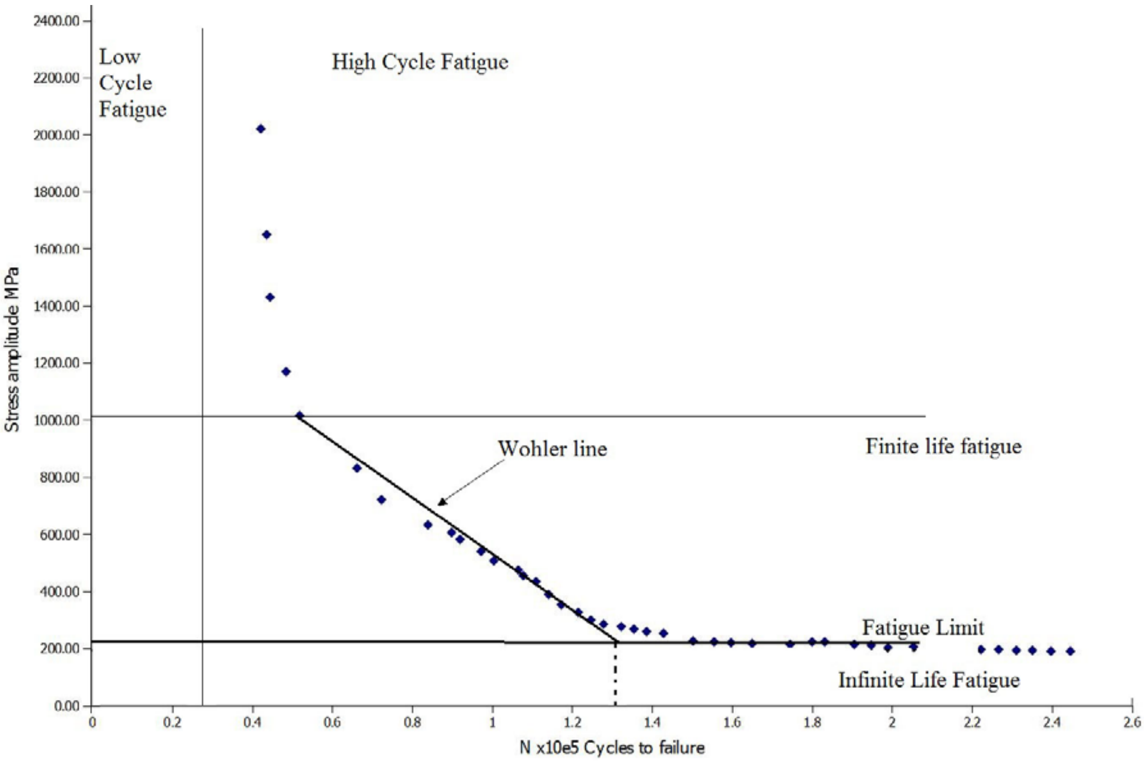

Figure 4. S-N curve for Al6061-9 % graphite, for T-S orientation.

Comparison with aluminium silicon carbide

In earlier works, the crack length and number of cycles are plotted for Al-TiC /37/, Al-SiC$_w$ /4/, Al6061 reinforced with silicon carbide and graphite particles /6/, Al-SiC /7-10, 17-22, 25/. The nature of variation of crack length and the number of cycles of Al6061-9 % graphite specimen is similar to the earlier works, as mentioned above.

The fatigue fracture behaviour of unreinforced aluminium alloy and aluminium composites is noticeably different. Figure 5 demonstrates the correlation of a crack growth profile on the surface of the specimen in unreinforced aluminium, Al-SiC, and Al-graphite composite. It is observed that the crack is moderately unrestricted in the unreinforced aluminium, while in the reinforced aluminium, the crack must pursue a convoluted way around the particles.

Additionally, Fig. 5 shows that the debonding of particle -matrix interface does not happen. Or maybe, the crack propagates a small, yet limited, distance far from the particle-matrix interface. This character has been affirmed by microstructure-based models that catch the genuine morphology and allocation of particles /35, 36/. It is likely associated with the modulus variance between SiC particles and the matrix.

The reinforcing particles act as an obstruction to the propagation of a crack in the matrix. Reinforcing particles reduce the stresses induced in the matrix, and also cause the deviation of the crack path as the crack deflects around the particles. The obstruction to crack propagation from reinforcement will increase the effect of roughness stimulated closure and consequently increase the limiting value for crack propagation.

Yury Flom et al. /35/ carried out an experimental investigation on the fracture behaviour of 40 % SiC/Al6061 MMC. From the obtained fatigue precracking data, the fatigue crack growth rate (FCGR) is estimated. From the results it is estimated that the threshold stress intensity of the material is $\Delta K_{th} = 2$ MPa$\sqrt{\text{m}}$ under which the crack would cease to grow.

Fatigue crack growth rate experiments are conducted on Al6061-9 % graphite. The threshold value at an $R = 0.1$ is determined to be between 3.5 to 3.75 MPa$\sqrt{\text{m}}$. Paris coefficients of Al6061-9 % graphite composite MMCs are determined using the fatigue crack growth rate vs. cyclic stress intensity factor (da/dN vs. ΔK) diagram. The best fitting line is drawn to the linear portion of the diagram, the Paris coefficients obtained are $C = 3.2344 \times 10^{-0.8}$ and $m = 1.07$.

(a)

(b)

(c)

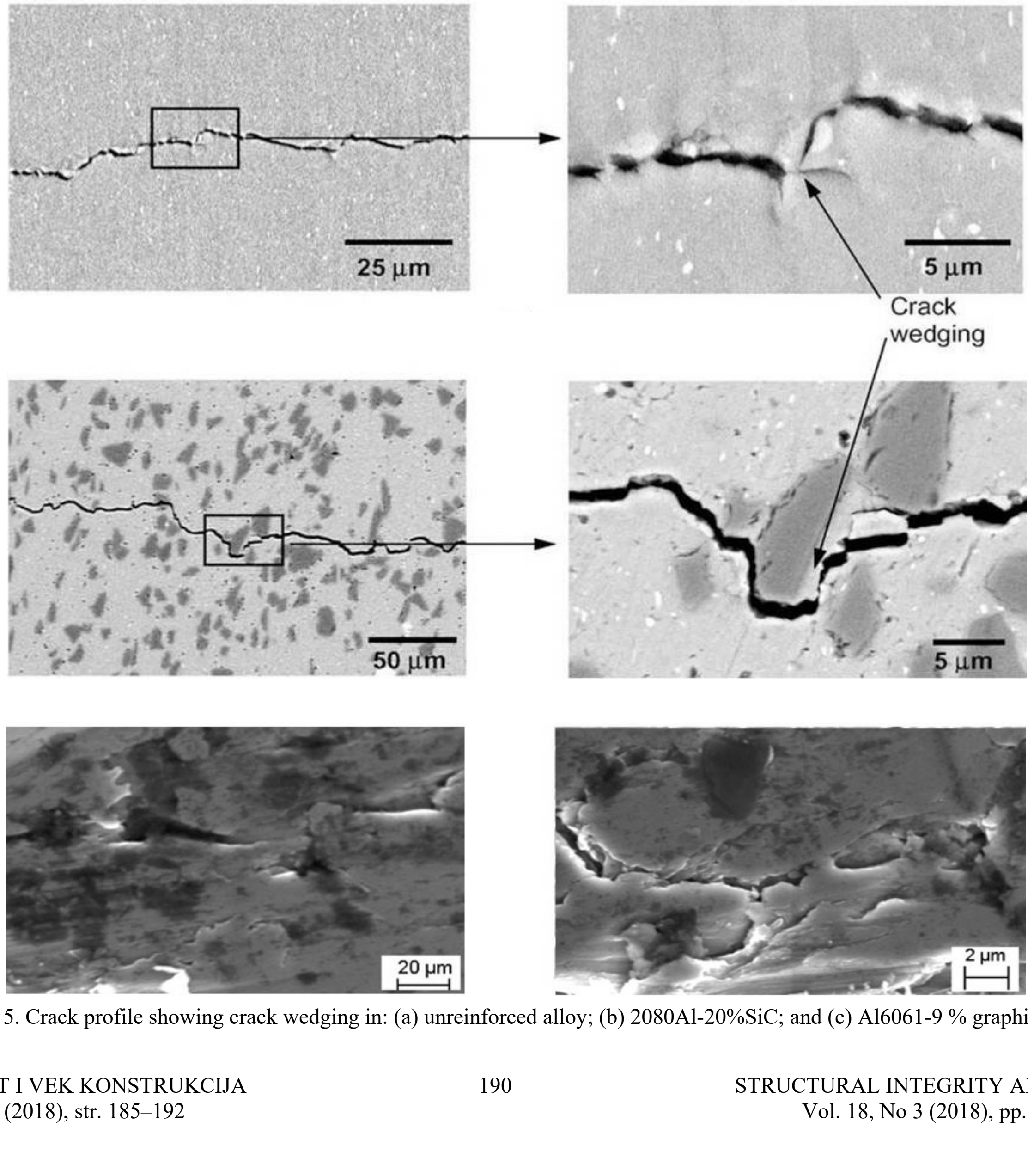

Figure 5. Crack profile showing crack wedging in: (a) unreinforced alloy; (b) 2080Al-20%SiC; and (c) Al6061-9 % graphite.

CONCLUSIONS

Fatigue crack growth rate (FCGR) experiments have been conducted for three different orientations, i.e. T-S, L-T, L-S. The CT specimens are utilized to evaluate the fatigue crack growth rate, fatigue life cycle estimation using the Paris equation. The threshold value at $R = 0$ is determined to be between 3.5 MPa√m to 3.75 MPa √m. The best fitting line is drawn to the linear portion of the diagram, the Paris coefficients obtained are $C = 3.2344 \times 10^{-0.8}$ and $m = 1.07$. From the trend of the S-N curve, it is found that the fatigue life of the MMC is reduced with increasing stress amplitude, for example, the fatigue life of the studied alloy is 2.1×10^5 under stress amplitude of 200 MPa, while about 1.30×10^5 under the stress amplitude of 250 MPa.

FUNDING

This research has received no specific grant from any funding agency in the public, commercial, or not-for-profit sectors.

REFERENCES

1. Anderson, T.L., Fracture Mechanics - Fundamentals and Applications. 3rd Ed., Taylor & Francis Group LLC, New York, 2005.
2. Xian-Kui Zhu, Joyce, J.A. (2012), *Review of fracture toughness (G, K, J, CTOD, CTOA) testing and standardization*, Eng. Frac. Mech., Elsevier, 85: 1-46. doi: 10.1016/j.engfracmech.2012.02.001
3. ASM Handbook Volume 21: Composites, ASM International, 2001.
4. Lee, E.E., Fatigue behavior of silicon carbide whisker/aluminum composite, Naval Air Development Center, Warminster, PA 18974-5000, Final Report, 1988.
5. Yuan, R., et al. (2003), *Ambient to high-temperature fracture toughness and cyclic fatigue behavior in Al-containing silicon carbide ceramics*, Science Direct, Acta Materialia 51: 6477-6491. doi: 10.1016/j.actamat.2003.08.038
6. Achutha, M.V., Sridhara, B.K., Abdul Budan, D. (2008), *Fatigue life estimation of hybrid aluminium matrix composites*, Int. J Design Manufact. Tech., 2(1): 14-21.
7. Uematsu, Y., Tokaji, K., Kawamura, M. (2008), *Fatigue behaviour of SiC-particulate-reinforced aluminium alloy composites with different particle sizes at elevated temperatures*, Compos. Sci. Tech. 68(13): 2785-2791. doi: 10.1016/j.compscitech.2008.06.005
8. Myriounis, D.P., Hasan, S.T. (2010), *Fatigue and fracture behaviour of Al-SiCp MMC NDE by IR detection*, ICCM 18th Int. Conf. Compos. Mater., 2010.
9. Huang, J., Spowart, J.E., Jones, J.W. (2010), *The role of microstructural variability on the very high-cycle fatigue behavior of discontinuously-reinforced aluminum metal matrix composites using ultrasonic fatigue*, Int. J Fatigue, 32(8): 1243-1254. doi: 10.1016/j.ijfatigue.2010.01.004
10. Sharma, M.M., et al. (2011), *Fatigue behavior of SiC particulate reinforced spray-formed 7XXX series Al-alloys*, Mater. and Design, 32(8): 4304-4309. doi: 10.1016/j.matdes.2011.04.009
11. Joadder, B., et al. (2011), *Fatigue failure of notched specimen - A strain-life approach*, Mater. Sci. Appl., 2(12): 1730-1740. doi: 10.4236/msa.2011.212231
12. Shahani, A.R., Kashani, H.M. (2013), *Assessment of equivalent initial flaw size estimation methods in fatigue life prediction using compact tension specimen tests*, Eng. Frac. Mech., 99: 48-61. doi: 10.1016/j.engfracmech.2013.01.007
13. Ciavarella, M. et al. (2017), *Generalized definition of 'crack-like' notches to finite life and SN curve transition from 'crack-like' to 'blunt notch' behavior*, Eng. Frac. Mech. 179: 154-164. doi: 10.1016/j.engfracmech.2017.04.048
14. Raposo, P., et al. (2017), *Probabilistic fatigue S-N curves derivation for notched components*, Frattura ed Integ. Strutt., 42: 105-118. doi: 10.3221/IGF-ESIS.42.12
15. Pugno, N., et al. (2006), *A generalized Paris' law for fatigue crack growth*, J Mech. Physics of Solids, 54: 1333-1349. doi: 10.1016/j.jmps.2006.01.007
16. Carpinteri, A., Paggi, M. (2007), *Are the Paris' law parameters dependent on each other?*, Fratt. ed Integ. Strutturale, 1(2): 10-16. doi: 10.3221/IGF-ESIS.02.02
17. Mohanty, J.R., Ray, P.K., Verma, B.B. (2010), *Determination of fatigue crack growth rate from experimental data: A new approach*, Int. J Microstr. Mater. Properties, 5(1): 79-87.
18. Davidson, D.L., Micromechanisms of Fatigue Crack Growth and Fracture Toughness in Metal Matrix Composites, Office of Naval Research, Tech Report, N00014-85-C-0206, 1989.
19. Mason, J.J., Ritchie, R.O. (1997), *Fatigue crack growth resistance in SiC particulate and whisker reinforced P/M 2124 aluminum matrix composites*, Mater. Sci. Eng., A231: 170-182.
20. Nirbhay Singh, et al. (2001), *Effect of stress ratio and frequency on fatigue crack growth rate of 2618 aluminium alloy silicon carbide metal matrix composite*, Bull. Mater. Sci., 24 (2): 169-171.
21. Li, X., et al. (2007), *High cycle fatigue and fracture behavior of 2124-T851 aluminum alloy*, Trans. Nonferrous Met. Soc. China, 17(2): 295-299.
22. Chawla, N., Ganesh, V.V. (2010), *Fatigue crack growth of SiC particle reinforced metal matrix composites*, Int. J Fatigue, 32(5): 856-863. doi: 10.1016/j.ijfatigue.2009.08.005
23. Gubeljak, N. et al. (2011), *CTOD-R curve construction from surface displacement measurements*, Eng. Frac. Mech. 78(11): 2286-2297. doi: 10.1016/j.engfracmech.2011.05.002
24. Han, K., et al. (2014), *The effect of constraint on CTOD fracture toughness of API X65 steel*, Eng. Frac. Mech., 124-125: 167-181. doi: 10.1016/j.engfracmech.2014.04.014
25. Hruby, P., et al. (2014), *Fatigue crack growth in SiC particle reinforced Al alloy matrix composites at high and low R-ratios by in situ X-ray synchrotron tomography*, Int. J Fatigue, 68: 136-143. doi: 10.1016/j.ijfatigue.2014.05.010
26. Souza, R.F. de, Ruggieri, C. (2017), *Revised wide range compliance solutions for selected standard and non-standard fracture test specimens based on crack mouth opening displacement*, Eng. Frac. Mech., 178: 77-92. doi: 10.1016/j.engfracmech.2017.04.013
27. Kawabata, T., et al. (2017), *Applicability of new CTOD calculation formula to various a_0/W conditions and $B \times B$ configuration*, Eng. Frac. Mech., 179: 375-390. doi: 10.1016/j.engfracmech.2017.03.027
28. Antunes, F.V., et al. (2017), *Effect of numerical parameters on plastic CTOD*, Fratt. Integ. Strutt., 41: 149-156. doi: 10.3221/IGF-ESIS.41.21
29. Vasco-Olmo, J.M., et al. (2017), *Experimental evaluation of CTOD in constant amplitude fatigue crack growth from crack tip displacement fields*, Fratt. Integ. Strutt., 41: 157-165. doi: 10.3221/IGF-ESIS.41.22
30. Cernescu, A. (2017), *The influence of crack tip shielding on fatigue crack propagation*, Fratt. Integ. Strutt., 11(41):307-313. doi: 10.3221/IGF-ESIS.41.41
31. Aluminum 6061-T6; 6061-T651 ASM Aerospace Specification Metals, Inc., 2015, www.aerospacemetals.com
32. Graphite (C)-Classifications, Properties and Applications of Graphite, Jul 12, 2013, CERAM Research Ltd.

33. Doddamani, S., Kaleemulla, M. (2017), *Experimental investigation on fracture toughness of Al6061-graphite by using circumferential notched tensile specimens*, Fratt. Integ. Strutt., 39: 274-281. doi: 10.3221/IGF-ESIS.39.25
34. Doddamani, S., Kaleemulla, M. (2017), *Fracture toughness investigations of Al6061-graphite particulate composite using compact specimens*, Fratt. Integ. Strutt., 41: 484-490. doi: 10.3221/IGF-ESIS.41.60
35. Flom, Y., Parker, B.H., Chu, H.P., Fracture toughness of SiC/Al metal matrix composite, NASA Technical Memorandum 100745, August 1989.
36. Ranjbaran, M.M. (2010), *Experimental investigation of fracture toughness in Al 356-SiCp aluminium matrix composite*, Am. J Sci. Ind. Res., 1(3): 549-557. doi: 10.5251/ajsir.2010.1.3.549.557
37. Raviraj, M.S., et al. (2016), *Experimental investigation of effect of specimen thickness on fracture toughness of Al-TiC composites*, Fratt. Integ. Strutt., 37: 360-368. doi: 10.3221/IGF-ESIS.37.47